Revised manuscript, submitted to J. Chem. Phys.

Elementary Steps of the Catalytic NO_x Reduction with NH_3: Cluster Studies on Adsorbate Diffusion and Dehydrogenation at Vanadium Oxide Substrate

M. Gruber and K. Hermann*

Inorg. Chem. Dept., Fritz-Haber-Institut der Max-Planck-Gesellschaft,
Faradayweg 4-6, 14195 Berlin, Germany

* Corresponding author, email: hermann@fhi-berlin.mpg.de

Subject classification: 68.43.-h, 68.47.Gh, 82.65.+r, 71.15.Mb, 68.43.Pq, 68.43.Bc, 68.43.Fg, 86.35.Fxm, 86.43.Jk

ABSTRACT

We discuss details of important steps of the selective catalytic reduction (SCR) of NO_x at model V_2O_5(010) substrate. First, diffusion processes at the substrate surface are considered where hydrogen and ammonium, NH_4, are used as examples. Hydrogen diffusion, a prerequisite for water formation involving substrate oxygen, is described by diffusion paths between adjacent surface oxygen sites. Corresponding energy barriers are determined mainly by the flexibility and the amount of distortion of the oxygen atoms which participate in the O-H-O bridge formation at the transition state. Further, diffusion of sub-surface oxygen to fill surface oxygen vacancies of the V_2O_5(010) substrate has been considered and results in reactive surface sites which have not been discussed so far. NH_4 diffusion at the V_2O_5(010) surface can be described as a combined tumbling and rotation process characterized by quite low diffusion barriers which make the adsorbate rather mobile. Finally, hydrogenation and dehydrogenation of different NH_x species at the V_2O_5(010) substrate surface are studied where special emphasis is given to the influence of surface reduction simulated locally by oxygen vacancies. The results confirm experimental findings of the presence of both NH_2 and NH_4 species after ammonia adsorption at the V_2O_5(010) surface.

1. INTRODUCTION

The selective catalytic reduction (SCR) of NO_x in the presence of ammonia is a complex reaction of great industrial importance[1]. It is applied, for example, in large stationary sources, such as fossil-fuel power plants, where NO_x species is removed from the exhaust gas to yield N_2 and H_2O with ammonia participating in the reduction according to

$$4\ NH_3 + 4\ NO + O_2 \rightarrow 4\ N_2 + 6\ H_2O \qquad (1)$$

or

$$4\ NH_3 + 2\ NO_2 + O_2 \rightarrow 3\ N_2 + 6\ H_2O \quad . \qquad (2)$$

Here TiO_2-supported V_2O_5-WO_3 and V_2O_5-MoO_3 catalysts are predominant in industrial applications[1-7]. Despite the technological importance of the SCR process at V_2O_5 based catalysts microscopic details, such as the nature of the active sites, are still under debate and various reaction mechanisms have been proposed in the literature, cp. Ref.[1] and references therein.

As discussed previously[8, 9], the SCR reaction can be considered, based on the experimental evidence, as consisting of three major parts

(i) The initial interaction and adsorption of gas phase NH_3 and NO resulting in different reaction species at the catalyst surface. Here relative surface binding energies of the adsorbate species have important implications for possible reaction mechanisms.

(ii) Adsorbate as well as surface oxygen diffusion. These processes determine to some extent the hydrogenation and dehydrogenation of NH_x surface species as well as surface water and oxygen vacancy formation, which contribute to the SCR reaction.

(iii) Interaction of the different adsorbates with the NO near the surface involving bond breaking / making. Here possible reaction scenarios can be already suggested by the findings in (i), (ii).

In our previous study[9] we focused on part (i) dealing with the adsorption and surface binding of atomic hydrogen, nitrogen, and oxygen, as well as molecular NO and NH_x, x = 1, … 4, adsorption at a model V_2O_5(010) substrate. Here we considered adsorption at different sites of the perfect crystalline substrate as well as at chemically reduced V_2O_5(010) sections where reduction is introduced by surface oxygen vacancies. These vacancies can be present as local perturbations which result, for example, from preceding oxidation reactions[1, 10-15] involving substrate oxygen in a

Mars-van-Krevelen type mechanism[16]. Our theoretical studies showed[8, 9] that surface reduction strongly affects the adsorption properties and reduced sites may play an important role for the SCR reaction. In particular, the adsorption of NH_3, believed to form the initial step of the SCR reaction, is found to be energetically favored at reduced vanadium sites (near oxygen vacancies) as compared with adsorption at vanadium sites of the perfect V_2O_5(010) substrate.

In the present theoretical study we discuss details of part (ii) of the SCR reaction referring to diffusion processes at the model V_2O_5(010) substrate. Here hydrogen and NH_4 surface species are used as examples where hydrogen diffusion is a prerequisite for water formation involving substrate oxygen and creating oxygen vacancies. Further, diffusion of sub-surface oxygen to fill surface oxygen vacancies of the V_2O_5(010) substrate needs to be considered and results in reactive surface sites which have not been discussed so far. Finally, we examine hydrogenation and dehydrogenation of different NH_x species at the V_2O_5(010) substrate surface where special emphasis is given to the influence of surface reduction. Specific reaction paths which may occur in the SCR reaction, part (iii) of the reaction scheme, have also been studied in detail[8] and will be published separately.

In Section 2 we introduce the models and describe computational methods while Section 3 presents results and discussion. Finally, Section 4 summarizes our conclusions.

2. THEORETICAL DETAILS

2.1 Geometry and Cluster Models

Here we restrict ourselves to a brief discussion of the local surface models used in this study while a more detailed account is presented Refs.[8, 9]. In the present work local surface regions of vanadia catalysts are modeled by those of the (010) surface of vanadium pentoxide, V_2O_5. This bulk material is described by a layer type orthorhombic lattice[17-19] with physical crystal layers, consisting of four oxygen and two vanadium planes each, parallel to (010) netplanes according to the nomenclature used e.g. in[17]. There are three different oxygen centers in each physical layer, terminal (vanadyl) oxygen, O(1), coordinated to one vanadium atom by a short bond ($d_{V\text{-}O}$ = 1.59 Å) and bridging oxygen, O(2) / O(3), coordinated to two or three vanadium atoms with V-O distances ranging between 1.78 Å and 2.02 Å. In the topmost layer at the V_2O_5(010) surface each of these differently coordinated oxygen species can point either inside the crystal or stick out of the

surface relative to the closest vanadium plane which results in six different types of oxygen. Here we denote oxygen pointing out of the surface by O(1), O(2), or O(3) while oxygen pointing into the bulk will be denoted by O(1'), O(2'), or O(3'), see Fig. 1a.

Local sections at the perfect V_2O_5(010) surface are modeled by reasonably large clusters cut out from one or two physical layers with experimental bulk positions for vanadium and oxygen[17-20]. Further, the electronic coupling of the local clusters with their atom environment of the V_2O_5 bulk (embedding) is simulated by saturating dangling bonds of peripheral oxygen atoms by hydrogen. This yields $V_aO_bH_c$ surface clusters differing in shape and size which depend on the specific local surface region to be modeled. In the present study, two additional clusters beyond those described in[9] are applied to model a specific surface NH_4 diffusion path, cluster $V_{14}O_{45}H_{20}$ of Fig. 1a, as well as the path of O(3') oxygen diffusing to a neighboring O(3) vacancy site, cluster $V_{16}O_{51}H_{24}$ of Fig. 1b. Further geometry details of the clusters are given in Refs.[8, 9]. In calculations of both adsorbate stabilization and diffusion processes selected oxygen and vanadium atoms close to the adsorbate (nearest and next nearest neighbors) are allowed to relax in response to the presence of the adsorbate.

2.2 Electronic Structure and Energetics

The electronic structure of the present clusters are evaluated within density-functional theory (DFT) using the cluster code StoBe[21] where the gradient corrected revised Perdew-Burke-Ernzerhof (RPBE) exchange-correlation functional[22-25] is applied. The Kohn-Sham orbitals are represented by linear combinations of atomic orbitals (LCAOs) using basis sets of contracted Gaussians as described in[8, 9].

The adsorption and binding of atoms and small molecules at the perfect and reduced vanadium oxide substrate is examined in total energy minimizations based on geometry optimizations of the adsorbates including corresponding substrate atoms. Transition states on vacancy and adsorbate diffusion paths between separated local equilibrium states are located using the nudged elastic band (NEB)[26-28] and the dimer method[29]. These methods are based on first order derivatives of the total energy. Therefore, corresponding saddle points on the potential energy surface characterizing transition states are verified by vibrational analyses. Atom charges of the clusters in their ground

and transition states are evaluated by Bader charge analyses[30] and will be referred to as atom charges *q* in the following. Further methodological details are discussed in Refs.[8, 9].

The present model studies are based exclusively on the use of the revised RPBE exchange-correlation functional[22-25] which has shown to yield rather reliable adsorption energies for oxygen and small molecules at metal surfaces[25]. As eluded earlier[9], the choice of gradient corrected functionals other than the presently applied RPBE approximation will affect the numerical results[31, 32]. It may even lead to somewhat different qualitative behavior of certain physical quantities as a result of general deficiencies of DFT to describe weak interactions and on-site Coulomb repulsion. However, we expect that the general physical trends concerning adsorbate geometries at the V_2O_5(010) surface and corresponding energetics will not be affected by the choice of the functional and are correctly described by the present treatment.

3. Results and Discussion

3.1. Adsorbate diffusion

The substrate surface, such as V_2O_5(010) can provide different adsorption sites and a molecule binding initially to one site may not react at the same site. Therefore, adsorbate diffusion processes are quite important for many surface reactions[33]. Considering the SCR reaction, diffusion properties of hydrogen and ammonium, NH_4, are of special interest. Hydrogen, which as a light atom may diffuse quite easily, is of general importance since it participates in many reaction steps of catalytic processes. Within the SCR process hydrogenation and dehydrogenation of ammonia contribute essential steps[1] requiring hydrogen to move between different adsorption sites. Further, the SCR process leads to water as a reaction product which is believed to be formed with oxygen from the catalyst substrate[34, 35]. This formation depends also on hydrogen diffusion at the substrate surface.

Many authors propose that during the SCR reaction a strongly bound NH_4 surface species, rather than NH_3, is the reacting partner of NO[1]. This raises the question whether NH_4 is mobile at the catalyst substrate or anchored at specific adsorption sites such that it cannot move. The analysis is particularly interesting in view of the fact that NH_4 is found to become a positively charged ion at

the V_2O_5(010) surface with electrostatic contributions as a result of charge - image charge interactions dominating the adsorptive binding[8, 9]. Both NH_4 and hydrogen bind quite strongly at the V_2O_5(010) surface. At the same time, their binding energies at different surface sites do not show major variations[8, 9]. Therefore, diffusion between adjacent sites may not require much energy depending on corresponding diffusion barriers which will be discussed in the following.

3.1.1. Hydrogen diffusion

At the perfect V_2O_5(010) surface hydrogen stabilizes at all five different oxygen sites where, as a result of H adsorption, local OH groups are formed[8, 9]. In contrast, hydrogen does not bind to vanadium sites of the surface. Therefore, hydrogen diffusion between adjacent oxygen sites can be viewed as an O-H bond breaking and making process. Here we distinguish between different regions of the V_2O_5(010) surface, the region along the ridge formed by the two adjacent rows of vanadyl oxygen O(1) (ridge region), that along the valley between adjacent ridges with bridging oxygen O(2) in its center (valley region), and that between ridges and valleys including vanadyl O(1) and triply bridging oxygen O(3), O(3') (slope region), see top of Fig. 2. Inside these regions all diffusion paths between adjacent oxygen sites have been evaluated. As a result, Fig. 2 shows at the top a set of paths A-B-…-K for hydrogen diffusing between oxygen sites of the V_2O_5(010) surface with equilibrium positions denoted by filled dots and transition state positions indicated by open circles. The bottom of Fig. 2 gives a graphical representation of the relative binding energies of hydrogen at corresponding equilibrium and transition state sites along the paths where the adsorption energy at the vanadyl site O(1) (site A in Fig. 2) is taken as the reference zero. Numerical values of the different energies are listed in Table 1 where

$$\Delta E(X \rightarrow Y) = E_{ads}(Y) - E_{ads}(X) \qquad (3)$$

is the difference between the hydrogen adsorption energies for the two equilibrium sites X, Y with X, Y denoting corresponding pairs of oxygen sites A, B, … K. Further, energies $D(X \rightarrow Y)$ and $D(Y \rightarrow X)$ refer to energy barriers for hydrogen diffusing from site X to Y and Y to X, respectively. Note that due to the symmetry of the V_2O_5(010) surface diffusion paths I → J and K → J connecting O(1) with O(2') sites are equivalent which holds also for diffusion paths D → E and G → F connecting O(3) with O(2) sites. Therefore, results for these equivalent paths are collected in the same entries in Table 1.

The computational results indicate that all diffusion paths follow the same basic mechanism. During the hydrogen diffusion from one oxygen site to the other an O-H-O bridge is formed in the transition state. The corresponding O-H distances of these bridges are quite similar and vary for different paths only slightly, between 1.2 Å and 1.3 Å, which, in each case, is marginally larger than the equilibrium distance at the initial oxygen site, 0.98 Å, but considerably smaller than the O-H distance between hydrogen at the initial site and the final oxygen site, see Table 2. This is illustrated in Fig. 3 where for each region an example path, B → C in the ridge, E → F in the valley, and G → H in the slope, is shown by its initial, transition, and final state geometry. The size of the corresponding energy barriers, see Fig. 2 and Table 1, is determined mainly by the flexibility and the amount of distortion of the oxygen atoms which participate in the O-H-O bridge formation at the transition state. As an example, Fig. 3a shows the diffusion of hydrogen between two adjacent oxygen sites B, C of the ridge with vanadyl oxygen O(1) being very flexible and easy to tilt. Thus, the corresponding barrier for path B → C is quite small, only 0.16 eV, and hydrogen can diffuse easily. In contrast, hydrogen diffusion between two neighboring oxygen sites O(2) in the valley, E, F, requires rather large V-O-V bond distortions in the transition state, see Fig. 3b, Therefore, the diffusion barrier for path E → F is large, 0.80 eV. The three-fold coordinated O(3) and O(3') atoms in the slope region are the least flexible at the V_2O_5(010) surface such that diffusion of hydrogen between these sites G, H is energetically most costly. Hence, the diffusion barrier for path G → H, see Fig. 3c, is the largest, 1.52 eV.

For hydrogen diffusion between vanadyl oxygen sites B and C at the vanadyl ridge two different diffusion paths have been found. The first, discussed above, describes a direct connection between sites B and C while the second can be characterized as a "detour" path where hydrogen diffuses from B to C via the bridging oxygen O(2') site between the two vanadyls O(1), see Figs. 1, 2. This O(2') site has been identified as a stable adsorption site for hydrogen[9]. However, the diffusion barrier between the O(1) and O(2') sites is much higher, 1.1 eV, see Table 1, compared with the barrier for direct O(1) → O(1) diffusion, 0.16 eV. Note that in Table 1 and Fig. 2 we discriminate between the two diffusion paths by using symmetry equivalent oxygen sites at the V_2O_5(010) surface, B equivalent with I and C equivalent with K. Then direct diffusion is considered as B ↔ C while detour diffusion as I ↔ J ↔ K with J characterizing the intermediate O(2') site.

Altogether, the evaluation of all relevant diffusion paths, see Table 1 and Fig. 2, suggests that hydrogen moves at the V_2O_5(010) surface most likely on top of the ridge which is energetically preferred.

3.1.2. Surface water formation

As a result of hydrogen diffusing between oxygen sites at the ridge of the V_2O_5(010) surface two hydrogen atoms may get close to each other and, together with their oxygen neighbors at the surface, may react to form surface water. As discussed in the last section hydrogen combines with the vanadyl oxygen species O(1) at the surface ridge to form stable OH groups, called O(1)H in the following. Two adjacent O(1)H groups can react with each other by transferring the hydrogen of one O(1)H to the other which leads to a bare vanadyl oxygen and a surface water species, $H_2O(1)$. The final state of this reaction

$$HO(1) + HO(1) \rightarrow H_2O(1) + O(1) \qquad (4)$$

is energetically lower than the initial state by only 0.07 eV from the present cluster calculations. Further, the computed energy barrier for this reaction amounts to 0.34 eV while the reverse process, surface water dissociation at O(1) to form two adjacent O(1)H groups, yields barrier of 0.41 eV. Both energy barriers are rather small and may easily be overcome such that surface water formation seems to be very likely to happen.

Reaction (4) is illustrated by Fig. 4 which shows the initial, transition, and final state geometries. Analogous to hydrogen diffusion between adjacent O(1) sites, cp. Fig.3a, the reaction path is characterized by a transition state where an O-H-O bridge is formed between the O(1) species and its adjacent O(1)H group with corresponding O-H distances of 1.15 Å and 1.33 Å, respectively, see Fig. 4. As before the two O(1) atoms can get close to each other by tilting due to their flexibility which explains the rather low reaction barrier. In the final state after $H_2O(1)$ formation the binding of the O(1) component with the vanadium below is weakened considerably. This is evident from an inspection of the V-O(1) distance which increases from 1.77 Å, with an O(1)H group, to 2.29 Å, with an $O(1)H_2$ group. (For comparison, the V-O(1) distance at the perfect V_2O_5(010) surface without hydrogen amounts to 1.59 Å.) At the same time, the vanadium atom below the $O(1)H_2$ binds with its $O(1)^*$ neighbor of the second physical layer underneath more strongly thereby reducing its V-$O(1)^*$ distance from 2.88 Å to 1.93 Å[8]. This is analogous to the formation of an oxygen vacancy $O(1)_{vac}$ where the V-$O(1)^*$ bond strengthening leads to a distance reduction from 2.88 Å to 1.77 Å[8].

The hydrogen induced V-O(1) bond weakening at the surface is obvious by considering the binding energy of the $O(1)H_2$ species with the surface which characterizes a possible water desorption process leaving an oxygen vacancy $O(1)_{vac}$ behind. Here the cluster calculations yield a barrier free desorption path with a binding energy (desorption energy) of only 0.44 eV which is similar to the formation barrier of $O(1)H_2$ at the surface. Thus, from an energetic point of view both processes, dissociation and desorption, are likely to occur. Previous theoretical studies on the desorption of surface water formed with O(1) oxygen yielded also barrier free desorption with energies of 0.56 eV[36] and 0.48 eV[37] which is quite close to the present value. These energies are considerably smaller than the vacancy formation energy at the O(1) site of the V_2O_5(010) surface, 4.98 eV[8, 9], which characterizes desorption of the O(1) surface species. This can also be interpreted as preadsorbed hydrogen at the V_2O_5(010) surface facilitating oxygen vacancy formation. This is in agreement with the experimental observations that oxygen vacancies are generated after the surface is exposed to atomic hydrogen[38] and that water is formed with surface oxygen during the SCR reaction[34, 35].

3.1.3. Ammonium diffusion

Ammonium, NH_4 is found to become positively charged at the V_2O_5(010) surface and its binding behavior is determined to a large extent by charge – image charge coupling[8, 9] which does not depend strongly on specific surface sites. Therefore, NH_4 can stabilize in different positions near all oxygen sites except for O(2'), where it does not fit between adjacent vanadyl groups O(1) due to its size, and it will also bind near vanadium sites of the surface[8, 9]. As a result of its size, NH_4 stabilizes at surface positions which involve usually several oxygen and/or vanadium sites and cannot be assigned uniquely to one atom site only. However, in the following we will still denote equilibrium positions of NH_4 at the V_2O_5(010) surface by one site considering the position of the nitrogen center. As before, we distinguish between different regions of the surface, ridge, valley, and slope in between, see top of Fig. 5. In these regions we identify different equilibrium positions where positions A and B (denoted O(1) in Table 3) refer to NH_4 above four O(1) sites of the ridge each, see Fig. 6a and 6c, respectively. Position C (denoted also O(1) in Table 3) refers to NH_4 in position B but rotated by about 30° about its surface normal, see Fig. 7c. Position D of the slope region (denoted V in Table 3) refers to NH_4 with its nitrogen center above a vanadium site while two of its hydrogen legs point towards O(1) sites and one towards O(2). Finally, position E of the

valley region (denoted O(2) in Table 3) refers to NH_4 near an O(2) site with two of its hydrogen legs pointing to vanadium atoms of the V-O(2)-V bridge, see Fig. 5. Positions $A^{(')}$ to $E^{(')}$ in Fig. 5 and Table 3 are symmetry equivalent with A to E and are added only for completeness.

Fig. 5 shows at the top a set of paths A-B-…-E-E'-D' …A' for ammonium diffusion connecting positions between two adjacent ridges of the V_2O_5(010) surface with equilibrium positions denoted by filled dots and transition state positions indicated by open circles. The bottom of Fig. 5 shows relative binding energies of NH_4 at corresponding equilibrium and transition state sites along the paths where the adsorption energy at the vanadyl site O(1) (site A in Fig. 5) is taken as the reference zero. Numerical values of the different energies are listed in Table 3 with definitions analogous to those for hydrogen diffusion, see Table 1 and Fig. 2.

Clearly, NH_4 diffusion between adjacent stable sites cannot be considered as a pure bond breaking and making process, as found for hydrogen diffusion, since NH_4 does not form strongly covalent bonds with the V_2O_5(010) surface. Yet, the electronic interaction of the hydrogen atoms in NH_4 with oxygen of the surface is strong enough such that, while diffusing, the NH_4 molecule tries to preserve coupling with to one or more oxygen sites. This leads to tumbling and rotation movements of the adsorbate at the surface. As an example, we consider NH_4 diffusion along the vanadyl ridge which is illustrated in Figs. 6, 7. Here example paths A → B (Fig. 6) and B → C (Fig. 7) are shown by their initial, transition, and final state geometries.

Starting from position A (Fig. 6a), where NH_4 sits above the square of four O(1) sites of the ridge with two of its hydrogen legs pointing to adjacent O(1) sites, the adsorbate tumbles over the two O(1) sites to reach position B of the adjacent square (Fig. 6c) with its two hydrogen legs still pointing at the same O(1) sites. In the transition state (Fig. 6b) NH_4 is positioned symmetrically above the two O(1) sites resulting in a diffusion barrier of only 0.17 eV. Interestingly, the transition state position, reflecting a saddle point in the potential energy surface (PES), has been considered in a number of studies[39-43] as an equilibrium position. This erroneous assignment is explained by the underlying PES being rather flat as indicated by the small energy barrier but also by the use of rather small substrate clusters[40, 42] which cannot account for the saddle point of the PES. Starting from position B, Figs.6c, 7a, the continued diffusion along the surface ridge requires NH_4 to rotate about the surface normal by 60° (twist movement) such that two of its hydrogen legs point towards the opposite O(1) pair of the square. This is achieved in two steps of rotations by 30° each where Fig. 7c shows the geometry after the first rotation step. The geometry of the corresponding

transition state reflects a rotation by about 15°, see Fig. 7b, and is connected with an extremely small energy barrier, below 0.002 eV, such that the adsorbate can rotate very easily. The second rotation by 30° is completely analogous to the first for symmetry reasons and is determined by the same extremely small energy barrier which concludes the twist motion. Altogether, combining tumbling and twist movements the NH_4 adsorbate can diffuse quite easily along the vanadyl row.

Analogous combinations of tumble and twist movements characterize the diffusion steps of NH_4 in the slope region, e. g. path C → D, and inside the valleys, paths D → E →E', of the V_2O_5(010) surface where energy barriers of corresponding transition states are always found to be rather low, below 0.3 eV, see Table 3 and Fig. 5. Thus, the calculations show that ammonium, while binding to the V_2O_5(010) surface quite strongly by mostly electrostatic coupling, is, at the same time, highly mobile and can diffuse easily at the surface.

3.2. Oxygen diffusion to nearby vacancies

In Sec. 3.1.2 we showed that, as a result of hydrogen diffusion and reaction at the V_2O_5(010) substrate, surface water can be formed and may easily desorb leaving an oxygen vacancy behind. On the other hand, the SCR of NO[44] and other catalytic processes, such as the oxidative dehydrogenation of hydrocarbons[14], are found to involve reduction of the substrate where oxygen vacancies are formed. Further, our theoretical studies on NH_3 adsorption[8, 9], believed to initiate the catalytic reduction of NO[1], showed that at the reduced V_2O_5(010) surface near oxygen vacancies NH_3 binds much more strongly than at vanadium sites of the perfect V_2O_5(010) surface. This must affect the catalytic process and oxygen vacancy properties need to be considered.

The actual distribution of different types of oxygen vacancies in V_2O_5 is still unclear. Scanning tunneling microscopy (STM) and angle-resolved X-ray photoelectron spectroscopy (ARXPS) experiments indicate that vacancies of vanadyl oxygen O(1) are most likely to occur[45-47]. This agrees with results from theoretical studies where strongly varying vacancy formation energies are found with that for O(1) being smallest[8, 9, 20, 31, 32, 37, 48-54]. In contrast, high resolution electron energy loss spectroscopy (HREELS) data suggests that O(2) vacancies are predominant[38] while ARUPS spectra indicate the presence of O(2) and/or O(3) vacancies[55].

During the SCR reaction the surface of the catalyst substrate must be re-oxidized by filling oxygen vacancies which can be achieved by molecular oxygen from gas phase. This was found to form an exothermic process involving per-oxo type surface species[20]. Alternatively, oxygen vacancies can be filled by diffusion of oxygen from nearby oxygen sites at the surface or in the substrate bulk as observed in isotopic labeling experiments[56]. This filling process may also be considered oxygen vacancy diffusion. The activation energy for vacancy diffusion was evaluated by classical kinetic models based on experimental data of oxygen chemisorption at V_2O_5 substrate[57] yielding 0.65 eV where, however, neither specific sites nor corresponding diffusion paths could be identified. So far, theoretical cluster studies have considered oxygen vacancy diffusion for selected model paths with geometric constraints that allow only an estimate of the upper limits of corresponding diffusion barriers[51]. Here a large range of barrier energies between 0.5 eV and 2.5 eV was found with the smallest barrier referring to oxygen diffusion from a vanadyl site O(1) to fill an O(2') vacancy and the largest barrier characterizing diffusion from O(2) to an O(3) vacancy.

In the present studies we have evaluated diffusion paths and energy barriers of oxygen diffusing from different sites to adjacent vacancies. For each diffusion path, corresponding differences ΔE in total energy between initial and final states, characterized by pairs of oxygen and oxygen vacancy sites, as well as diffusion energies D for both path directions are listed in Table 4. An analysis of the different paths shows clearly that oxygen diffusion is always accompanied by sizeable relaxation of the surrounding V/O network of the substrate. This facilitates the diffusion process and lowers corresponding barriers. It explains why the energies D of the diffusion barriers given in Table 4 are overall considerably smaller than the values obtained in Ref.[51] from approximate model paths ignoring substrate relaxation.

Fig. 8 shows as an example the energetics along the diffusion path of oxygen from an O(3') site to a neighboring vacancy site $O(3)_{vac}$, see Fig. 1. The figure includes also sketches of corresponding initial (denoted $O(3')/O(3)_{vac}$), transition, and final state geometries (denoted $O(3)/O(3')_{vac}$). Here the oxygen, initially binding with three vanadium neighbors, breaks one V-O bond and "squeezes" between two vanadium neighbors which, in response, move apart by about 0.2 Å in the transition state geometry. This is documented in Fig. 8 by V-O distances a, b between the diffusing oxygen and its vanadium neighbors. As a consequence of relaxation, the corresponding diffusion energy barriers are rather moderate, 0.44 eV, see Table 4.

Fig. 9 shows the energetics along the diffusion path of oxygen from a sub-surface O(1') site to a neighboring vacancy site $O(2)_{vac}$, see Fig. 1, where sketches of corresponding initial (denoted $O(1')/O(2)_{vac}$), transition, and final state geometries (denoted $O(2)/O(1')_{vac}$) are included. In this example the diffusing oxygen atom, initially binding to one vanadium atom in a vanadyl double bond, bends towards the O(2) vacancy where it forms single bonds with two vanadium neighbors. This is characterized by an extremely small barrier of only 0.08 eV, see Table 4 while the energy gain after diffusion is rather large, 0.85 eV. It shoes that oxygen diffusion from O(1') to $O(2)_{vac}$ is a highly exothermic process and very likely to occur. Similar findings are obtained for oxygen diffusion from O(1) to $O(2')_{vac}$ with even higher energy gain and almost no barrier. Based on these theoretical results, the stability of oxygen vacancies $O(2)_{vac}$ and $O(2')_{vac}$ that have been suggested by experimentalists to be the predominant species[38, 55] is questionable.

As a result of oxygen diffusing easily from sub-surface O(1') sites to adjacent surface vacancies, sub-surface vacancies $O(1')_{vac}$ seem to be very likely to occur in the reacting $V_2O_5(010)$ substrate. This will reduce corresponding surface vanadium atoms above the vacancy sites $O(1')_{vac}$ leading to rather reactive $V/O(1')_{vac}$ Lewis acid sites which can participate in the catalytic reduction of NO. Therefore, sub-surface O(1') vacancies have to be taken into account in a full description of the reduction process as will be discussed separately[58].

3.3. NH_x hydrogenation and dehydrogenation

Experiments examining the SCR reaction detect NH_3 and NH_4 species[1, 59] as well as giving clear indications for the presence of NH_2[59, 60] at the catalyst surface. Thus, reaction schemes of the SCR reaction must include NH_x hydrogenation and dehydrogenation steps as discussed earlier[1, 8, 9] and the ability of the catalyst to (de)hydrogenate NH_x species is important for its catalytic performance. In the following, we compare NH_x (de)hydrogenation reactions in gas phase with those at the $V_2O_5(010)$ model surface where we consider both reactions at the perfect surface and at different oxygen vacancy sites of the reduced surface.

The present discussion is based on reaction energies, E_R, that represent thermodynamic limits taking into account only energies at the initial and at the final state of the reaction, thus, ignoring information about possible diffusion and reaction barriers. If the binding energy $E_B(x)$ of a hydrogen atom in NH_x is given by

$$E_B(x) = E_{tot}(NH_{x-1}) + E_{tot}(H) - E_{tot}(NH_x) \quad (6)$$

then the dehydrogenation energy $E_R^g(x)$ of a reaction

$$NH_x \rightarrow NH_{x-1} + ½H_2 \quad (7)$$

in gas phase defined with respect to atoms in molecular hydrogen, H_2, can be written as

$$E_R^g(x) = E_B(x) - ½ E_B(H_2) \quad (8)$$

where

$$E_B(H_2) = 2 E_{tot}(H) - E_B(H_2) \quad (9)$$

is the binding energy of molecular hydrogen. Results for calculated binding energies $E_B(x)$ and $E_B(H_2)$ are listed in Table 5 and compared with experimental data. Overall, the agreement between theory and experiment is rather satisfactory and the trend towards larger binding energies by increasing the size of the NH_x molecule from x = 1 to x = 3 is nicely reproduced. The theoretical hydrogen binding energy of NH_4 cannot be compared with experiment since NH_4 is not available in gas phase.

Reaction energies for dehydrogenation of NH_x at the catalyst surface can be obtained in a gedanken experiment applying a Born-Haber cycle[63] where the NH_x molecule is first desorbed from the surface. Then the dehydrogenation is performed in gas phase after which the reaction products adsorb at the surface. This leads to a dehydrogenation energy $E_R^s(x)$

$$E_R^s(x) = E_B(x) - E_{ads}(NH_x) + E_{ads}(NH_{x-1}) + E_{ads}(H) \quad (10)$$

where $E_{ads}(NH_x)$, $E_{ads}(NH_{x-1})$, and $E_{ads}(H)$ are corresponding adsorption energies of the different species which have been evaluated earlier for both perfect and reduced $V_2O_5(010)$ surfaces modeled by the presence of oxygen vacancies[8, 9]. Table 6 compares the theoretical gas phase values, $E_R^g(x)$ according to (8), with values of $E_R^s(x)$ according to (10) for the perfect $V_2O_5(010)$ surface as well as for different oxygen vacancy sites of the reduced surface. Here the adsorption energies $E_{ads}(NH_x)$ for the surface are assumed to refer always to the energetically most favorable adsorption site. Fig. 10 shows the $E_R^g(x)$ and $E_R^s(x)$ data of Table 6 in an energy level diagram where all energies are given relative to the value $E_R^s(x=3)$ of NH_3 at the surface (the initiating adsorbate species for the SCR reaction) which set to zero.

The theoretical results of Table 6 and Fig. 10 show that in gas phase the dehydrogenation of NH_x, x = 1, … 3, is always highly endothermic which is also found for the hydrogenation of

ammonia. The presence of the perfect V_2O_5(010) surface lowers all dehydrogenation energies with respect to those in gas phase which can be considered a catalytic effect due to the binding of the different NH_x species and hydrogen at the surface. However, the dehydrogenation reactions steps are still rather endothermic. In contrast, the hydrogenation of NH_3 becomes exothermic as a result of the strong surface binding of the NH_4 species which is consistent with the presence of adsorbed NH_4 found in experiment[59, 64]. However, the theoretical result that NH_4 at the perfect surface is energetically more favorable than NH_3 which seems to contradict the experimental findings[59, 64]. When adsorbed NH_x species near oxygen vacancies at the reduced V_2O_5(010) surface is included the dehydrogenation of NH_x is even less endothermic and near oxygen vacancies $O(2)_{vac}$ and $O(3)_{vac}$ ammonia dehydrogenation becomes an exothermic reaction. This is compatible with the experimentally verified presence of NH_2 at vanadia substrate after ammonia adsorption[59, 60]. Further, near vanadyl oxygen vacancies $O(1)_{vac}$ and at vanadium sites V/O(1') above sub-surface vacancies $O(1)_{vac}$ the hydrogenation of ammonia to yield surface NH_4 species is only slightly exothermic (compared with large exothermicity at the perfect surface). This can explain the experimental observation that the two surface species, NH_3 and NH_4, coexist during the SCR reaction[1, 59, 64]. Finally, the theoretical results for dehydrogenation of NH yield, in all cases, endothermic processes where the endothermicity is larger for the reduced than for the perfect surface. This suggests that the production of surface nitrogen by successive dehydrogenation of NH_3 is thermodynamically hindered which is consistent with the experimental findings of only NH_2, NH_3, and NH_4 species at the surface[1, 59, 60, 64].

4. Conclusions

The present cluster model studies build on our previous work where we have studied adsorption properties, geometric, energetic, and electronic quantities, of different adsorbate species that can occur at a vanadium oxide surface where the selective catalytic reduction (SCR) of NO in the presence of ammonia proceeds[8, 9]. Here we consider further processes which represent important steps of the SCR reaction, diffusion of selected adsorbates and of oxygen where paths and energetics of the diffusing surface species are examined at local sections of the vanadium oxide surface. In addition, we report results from cluster calculations referring to hydrogenation and dehydrogenation of different NH_x species at the V_2O_5(010) substrate surface where special emphasis is given to the influence of surface reduction simulated locally by oxygen vacancies. All

surface sections are modeled by sufficiently large clusters with their electronic structure described by DFT methods.

As a result of hydrogen stabilizing exclusively at the differently coordinated oxygen sites of the perfect V_2O_5(010) surface forming stable OH groups, hydrogen diffusion is described as a bond-braking-and-making process by paths between adjacent surface oxygen sites. Here transition states are characterized by O-H-O bridges with O-H distances that are quite similar and vary for different paths only slightly. The size of corresponding energy barriers is determined mainly by the flexibility and the amount of distortion of the participating oxygen atoms in the transition state. Thus, hydrogen diffusion along rows of flexible vanadyl oxygen sites O(1) is more likely to happen (barrier energies of 0.2 eV to 0.4 eV) than between more rigid bridging O(2) or O(3) sites. Hydrogen diffusion between oxygen sites can lead to two hydrogen atoms getting close to each other and, together with their oxygen neighbors at the surface, the hydrogen may react to form surface water. This reaction has been analyzed in detail at vanadyl oxygen sites. The theoretical results yield rather small energy barriers, 0.3 eV, for the surface water formation. Further, the binding of two hydrogen atoms at the O(1) site weakens the corresponding O(1)-V bond considerably such that desorption of surface water becomes quite easy with theoretical desorption energies amounting to only 0.4 eV. Thus, from an energetic point of view both processes, surface water formation and desorption, are very likely to occur.

Ammonium, NH_4, which becomes positively charged at the V_2O_5(010) surface, can stabilize near all oxygen and vanadium sites with fairly large binding energies and its binding behavior depending only little on specific sites due to its dominantly electrostatic coupling with the surface[8, 9]. Therefore, NH_4 diffusion cannot be described as an obvious bond-braking-and-making process and the PES for NH_4 moving at the V_2O_5(010) surface is found to be rather flat. As a consequence, diffusion barriers between equilibrium configurations of adsorbed NH_4 are quite low, only 0.1 eV to 0.3 eV, such that NH_4 can diffuse quite easily making it rather mobile. Corresponding minimum energy paths of the tetrahedral adsorbate are described as combinations of tumble and twist movements.

During the SCR process the surface of the catalyst substrate must be re-oxidized by filling oxygen vacancies. This can be achieved by either molecular oxygen from gas phase or by diffusion of oxygen from nearby oxygen sites at the surface or in the substrate bulk which may also be considered as oxygen vacancy diffusion. Corresponding paths and energy barriers of oxygen

diffusing from different sites to adjacent vacancies show clearly that oxygen diffusion is always accompanied by sizeable relaxation of the surrounding V/O network of the substrate. This facilitates the diffusion process and lowers corresponding barriers. The contribution of substrate relaxation can explain why the present diffusion barriers are, overall, much smaller than those obtained earlier[51] without substrate relaxation. Further, oxygen from sub-surface sites of the substrate is found to diffuse easily to the surface resulting in rather reactive vanadium Lewis acid sites which can participate in the catalytic reduction and have not been discussed so far.

Another component of the SCR process is the hydrogenation and dehydrogenation of different NH_x species at the V_2O_5(010) substrate surface. Here comparisons of NH_x (de)hydrogenation reactions in gas phase with those at the V_2O_5(010) model surface, where both reactions at the perfect surface and at different oxygen vacancy sites of the reduced surface are considered, give a clear picture. In gas phase, hydrogen binding energies of NH_x are always quite large yielding strongly endothermic dehydrogenation reactions for NH_x, x = 1, 2, 3, which is also found for NH_3 hydrogenation. Reaction energies at the perfect V_2O_5(010) surface, evaluated using Born-Haber cycles, are smaller than corresponding gas phase results and the NH_3 hydrogenation reaction becomes exothermic while the NH_x dehydrogenation reactions are still endothermic. If (de)hydrogenation is modeled near oxygen vacancies of the reduced V_2O_5(010) surface the NH_x dehydrogenation energies are further decreased and the NH_3 dehydrogenation may even become exothermic. Clearly, the model results can only give a qualitative estimate since the energy analysis is based only on equilibrium energies of the different species which ignores barrier energies of corresponding reaction paths. However, the present simulation of the catalytic effect of the vanadium oxide surface supports the experimental findings of NH_4 as well as NH_2 species after ammonia adsorption at the surface[59, 60, 64].

Altogether, the different diffusion processes, considering both adsorbed reactants and substrate oxygen, as well as NH_x (de)hydrogenation at the vanadium oxide substrate can give further insight into details of SCR process. As a next step, the adsorption and reaction of NO from gas phase with the NH_3 adsorbate needs to be examined. Here it has been suggested from experiment[1, 65, 66] and theory[39, 40, 42, 67-70] that the reaction proceeds via a nitrosamide, NH_2NO, intermediate at the substrate surface. Based on our previous work on NH_3 adsorption[8, 9] and the present diffusion results, two different reaction scenarios are conceivable. First , NO may react with NH_4 surface species resulting from NH_3 adsorbed at an OH group (Brønsted acid site) of the perfect vanadium

oxide substrate. Second, NO may interact with NH_3 adsorbed at an oxygen vacancy site of the reduced substrate. Both, scenarios will be discussed in great detail in a forthcoming publication[58].

5. Acknowledgements

M. G. is grateful for continued support by the International Max-Planck Research School (IMPRS) “Complex Surfaces in Materials Science” in Berlin. Financial support by the German Research Foundation (DFG) via its Joint Collaborative Research Center, Sfb 548 “Structure, Dynamics, and Reactivity of Transition Metal Oxide Aggregates”, is greatly acknowledged. K. H. is grateful for financial support by the Institute of Computational and Theoretical Studies, Hong Kong Baptist University, where part of this manuscript was completed.

References

[1] G. Busca, L. Lietti, G. Ramis, and F. Berti, Appl. Catal. B: Environmental **18**, 1 (1998).

[2] L. J. Alemany, F. Berti, G. Busca, G. Ramis, D. Robba, G. P. Toledo, and M. Trombetta, Appl. Catal. B **10**, 299 (1996).

[3] H. Bosch and F. J. Janssen, Catal. Today **2**, 369 (1988).

[4] S. M. Cho, Chem. Eng. Prog. **90**, 39 (1994).

[5] P. Forzatti and L. Lietti, Heterogen. Chem. Rev. **3**, 33 (1996).

[6] F. J. J. G. Janssen, in *Handbook of Heterogeneous Catalysis*, ed. by G. Ertl, H. Knötzinger, J. Weitkamp (Wiley-VCH, Weinheim, 1997).

[7] S. C. Wood, Chem. Eng. Prog. **90**, 33 (1994).

[8] M. Gruber, Ph.D. dissertation, Freie Universität Berlin, Berlin, 2012.

[9] M. Gruber and K. Hermann, J. Chem. Phys. **138**, 094704 (2013).

[10] K. Chen, E. Iglesia, and A. T. Bell, J. Catal. **192**, 197 (2000).

[11] K. Chen, A. Khodakov, J. Yang, A. T. Bell, and E. Iglesia, J. Catal. **186**, 325 (1999).

[12] R. K. Grasselli, Top. Catal. **21**, 79 (2002).

[13] J. Haber, "*Fundamentals of Hydrocarbon Oxidation"* in *Handbook of Heterogeneous Catalysis* (Wiley-VCH, Weinheim, 2008).

[14] M. E. Harlin, V. M. Niemi, and A. O. I. Krause, J. Catal. **195**, 67 (2000).

[15] B. Weckhuysen, Catal. Today **78**, 25 (2003).

[16] P. Mars and D. W. van Krevelen, Chem. Eng. Sci. **3**, 41 (1954).

[17] H. G. Bachmann, F. R. Ahmed, and W. H. Barnes, Z. Kristallogr. **115**, 110 (1961).

[18] A. Byström, K.-A. Wilhelmi, and O. Brotzen, Acta Chem. Scand. **4**, 1119 (1950).

[19] R. W. G. Wyckoff, *Crystal Structures* (Interscience, Wiley, New York, 1965).

[20] K. Hermann and M. Witko, "*Theory of physical and chemical behavior of transition metal oxides: vanadium and molybdenum oxides"* in *The Chemical Physics of Solid Surfaces*, edited by D. P. Woodruff (Elsevier, 2001), pp. 136.

[21] K. Hermann and L. G. M. Pettersson, deMon developers group, StoBe software V. 3.6, 2012, see http://www.fhi-berlin.mpg.de/KHsoftware/StoBe/.

[22] J. P. Perdew, K. Burke, and M. Ernzerhof, Phys. Rev. Lett. **77**, 3865 (1996).

[23] J. P. Perdew, K. Burke, and M. Ernzerhof, Phys. Rev. Lett. **78**, 1396 (1997).

[24] J. P. Perdew, K. Burke, and Y. Wang, Phys. Rev. B **54**, 16533 (1996).

[25] B. Hammer, L. B. Hansen, and J. K. Nørskov, Phys. Rev. B **59**, 7413 (1999).

[26] G. Mills, H. Jónsson, and G. K. Schenter, Surf. Sci. **324**, 305 (1995).

[27] G. Mills and H. Jónsson, Phys. Rev. Lett. **72**, 1124 (1994).

[28] H. Jónsson, G. Mills, and K. W. Jacobson, "*Nudged elastic band metthod for finding minimum energy paths and transitions"* in *Classical and Quantum Dynamics in Condensed Phase Simulations*, edited by B. J. Berne, G. Ciccotti, and D. F. Coker (World Scientific Publishing Company, 1998).

[29] G. Henkelman and H. Jónsson, J. Chem. Phys. **111**, 7010 (1999).

[30] R. F. W. Bader, *Atoms in Molecule, A Quantum Theory* (Clarendon Press, Oxford, 1990), Vol. 22, International Series of Monographs on Chemistry.

[31] J. Sauer and J. Dobler, Dalt. Trans. 3116 (2004).

[32] D. O. Scanlon, A. Walsh, B. J. Morgan, and G. W. Watson, J. Phys. Chem. C **112**, 9903 (2008).

[33] J. A. Dumesic, G. W. Huber, and M. Boudart, "*Rates of Catalytic Reactions"* in *Handbook of Heterogeneous Catalysis* (Wiley-VCH, Weinheim, 2008).

[34] F. J. J. G. Janssen, F. M. G. Van den Kerkhof, H. Bosch, and J. R. H. Ross, J. Phys. Chem. **91**, 5921 (1987).

[35] F. J. J. G. Janssen, F. M. G. Van den Kerkhof, H. Bosch, and J. R. H. Ross, J. Phys. Chem. **91**, 6633 (1987).

[36] H. Fu, Z.-P. Liu, Z.-H. Li, W.-N. Wang, and K.-N. Fan, J. Am. Chem. Soc. **128**, 11114 (2006).

[37] K. Hermann, M. Witko, R. Družinić, and R. Tokarz, Top. Catal. **11-12**, 67 (2000).

[38] B. Tepper, B. Richter, A. C. Dupuis, H. Kuhlenbeck, C. Hucho, P. Schilbe, M. A. bin Yarmo, and H. J. Freund, Surf. Sci. **496**, 64 (2002).

[39] M. Anstrom, N.-Y. Topsøe, and J. A. Dumesic, J. Catal. **213**, 115 (2003).

[40] F. Gilardoni, J. Weber, and A. Baiker, Int. J. Quantum Chem **61**, 683 (1997).

[41] T. Homann, T. Bredow, and K. Jug, Surf. Sci. **515**, 205 (2002).

[42] S. Soyer, A. Uzun, S. Senkan, and I. Onal, Catal. Today **118**, 268 (2006).

[43] X. Yin, H. Han, I. Gunji, A. Endou, S. S. Cheettu Ammal, M. Kubo, and A. Miyamoto, J. Phys. Chem. B **103**, 4701 (1999).

[44] M. Inomata, A. Miyamoto, and Y. Murakami, J. Catal. **62**, 140 (1980).

[45] R. L. Smith, W. Lu, and G. S. Rohrer, Surf. Sci. **322**, 293 (1995).

[46] T. Oshio, Y. Sakai, and S. Ehara, J. Vac. Sci. Technol. B **12**, 2055 (1994).

[47] K. Devriendt, H. Poelman, L. Fiermans, G. Creten, and G. F. Froment, Surf. Sci. **352-354**, 750 (1996).

[48] R. Družinić, Ph.D. dissertation, Freie Universität Berlin, Berlin, 1999.

[49] C. Friedrich, Ph.D. dissertation, Freie Universität Berlin, Berlin, 2004.

[50] K. Hermann, M. Witko, and R. Družinić, Faraday Discuss. **114**, 53 (1999).

[51] K. Hermann, M. Witko, R. Družinić, and R. Tokarz, Appl. Phys. A **72**, 429 (2001).

[52] M. Ganduglia-Pirovano and J. Sauer, Phys. Rev. B **70**, 045422 (2004).

[53] J. Goclon, R. Grybos, M. Witko, and J. Hafner, Phys. Rev. B **79**, 075439 (2009).

[54] S. Laubach, P. C. Schmidt, A. Thißen, F. J. Fernandez-Madrigal, Q.-H. Wu, W. Jaegermann, M. Klemm, and S. Horn, PCCP **9**, 2564 (2007).

[55] K. Hermann, M. Witko, R. Družinić, A. Chakrabarti, B. Tepper, M. Elsner, A. Gorschlüter, H. Kuhlenbeck, and H. J. Freund, J. Electron. Spectrosc. Relat. Phenom. **98-99**, 245 (1999).

[56] E. R. S. Winter, J. Chem. Soc. A 2889 (1968).

[57] N. E. Quaranta, L. A. Gambaro, and H. J. Thomas, J. Catal. **107**, 503 (1987).

[58] M. Gruber and K. Hermann, J. Chem. Phys. (2013) to be submitted.

[59] G. Ramis, L. Yi, and G. Busca, Catal. Today **28**, 373 (1996).

[60] M. S. Went and J. A. Reimer, J. Am. Chem. Soc. **114**, 5768 (1992).

[61] G. Ertl, in *Catalysis Science and Technology Vol. 4*, edited by J. R. Anderson, and M. Boudart (Springer, Berlin, 1983), p. 209.

[62] L. V. Gurvich, I. V. Veyts, C. B. Alcock, and V. S. Iorish, *Thermodynamic Properties of Individual Substances* (Hemisphere, New York, 1991), 4th edn., Vol. 2.

[63] F. Haber, Verhandlungen der Deutschen Physikalischen Gesellschaft **21**, 750 (1919).

[64] Y. V. Belokopytov, K. M. Kholyavenko, and S. V. Gerei, J. Catal. **60**, 1 (1979).

[65] G. Ramis, G. Busca, F. Bregani, and P. Forzatti, Appl. Catal. **64**, 259 (1990).

[66] M. Farber and S. P. Harris, J. Phys. Chem. **88**, 680 (1984).

[67] R.-M. Yuan, G. Fu, X. Xu, and H.-L. Wan, PCCP **13**, 453 (2011).

[68] A. Vittadini, M. Casarin, and A. Selloni, J. Phys. Chem. B **109**, 1652 (2005).

[69] E. W.-G. Diau and S. C. Smith, J. Chem. Phys. **106**, 9236 (1997).

[70] X. Duan and M. Page, J. Mol. Struct. TEOCHEM **333**, 233 (1995).

Tables

Table 1

Energetics for hydrogen diffusion between different oxygen sites A … K at the V_2O_5(010) surface, see Fig. 2. The pairs X, Y define diffusion paths between two oxygen sites O(1), O($2^{(\prime)}$), or O($3^{(\prime)}$) each as given in the Table. For each path of the ridge, slope, and valley region corresponding differences ΔE in adsorption energy and diffusion energies D for both path directions are listed, see text. All energies are shown in eV.

X - Y	Sites	ΔE(X→Y)	D(X→Y)	D(Y→X)
Ridge				
A - B	O(1) - O(1)	0.00	0.43	0.43
B - C	O(1) - O(1)	0.00	0.16	0.16
I – J, K - J	O(1) - O(2')	0.07	1.14	1.08
Slope				
C -D	O(1) - O(3)	0.11	1.20	1.09
G - H	O(3) - O(3')	0.19	1.52	1.34
H - I	O(3') - O(1)	-0.25	1.00	1.25
Valley				
D - E, G - F	O(3) - O(2)	-0.19	0.64	0.83
E - F	O(2) - O(2)	0.00	0.80	0.80

Table 2

OH distances for hydrogen diffusion between different oxygen sites A … K at the V_2O_5(010) surface, see Fig. 2. The pairs X, Y define diffusion paths between two oxygen sites O(1), O($2^{(\prime)}$), or O($3^{(\prime)}$) each as given in the Table. For each path of the ridge, slope, and valley region corresponding OH distances $d_{X\text{-}H}$ / $d_{Y\text{-}H}$ are listed for hydrogen adsorbed at X, the transition state, and hydrogen adsorbed at Y, see text. (Calculated gas phase values of $d_{O\text{-}H}$ are 0.98 Å for free OH and 0.97 Å for free H_2O.) All distances in the Table are given in Å.

X - Y	**Sites**	**H at X** $\mathbf{d_{X\text{-}H}}$ **/** $\mathbf{d_{Y\text{-}H}}$	**TS** $\mathbf{d_{X\text{-}H}}$ **/** $\mathbf{d_{Y\text{-}H}}$	**H at Y** $\mathbf{d_{X\text{-}H}}$ **/** $\mathbf{d_{Y\text{-}H}}$
Ridge				
A - B	O(1) - O(1)	0.98 / 3.82	1.23 / 1.22	3.82 / 0.98
B - C	O(1) - O(1)	0.99 / 2.17	1.22 / 1.22	2.17 / 0.99
I – J, K - J	O(1) - O(2’)	0.99 / 2.63	1.22 / 1.33	2.36 / 0.98
Slope				
C -D	O(1) - O(3)	0.98 / 3.92	1.25 / 1.28	3.06 / 0.98
G - H	O(3) - O(3’)	0.98 / 3.04	1.23 / 1.24	2.78 / 0.97
H - I	O(3’) - O(1)	0.97 / 2.50	1.28 / 1.24	3.48 / 0.98
Valley				
D - E, G - F	O(3) - O(2)	0.98 / 2.47	1.24 / 1.25	2.38 / 0.98
E - F	O(2) - O(2)	0.98 / 2.85	1.26 / 1.27	2.58 / 0.98

Table 3

Energetics for NH_4 diffusion between different oxygen sites $A^{(,)}$ … $E^{(,)}$ at the V_2O_5(010) surface, see Fig. 5. The pairs X, Y define diffusion paths between oxygen and vanadium sites O(1), O($2^{(,)}$), or V each as given in the Table. For each path of the ridge, slope, and valley region corresponding differences ΔE in adsorption energy and diffusion energies D for both path directions are listed, see text. All energies are shown in eV.

X - Y	**Sites***	**ΔE(X→Y)**	**D(X→Y)**	**D(Y→X)**
Ridge				
$A^{(,)}$ - $B^{(,)}$	O(1) - O(1)	0.00	0.17	0.17
$B^{(,)}$ - $C^{(,)}$	O(1) - O(1)	0.001	0.002	0.001
Slope				
$C^{(,)}$ -$D^{(,)}$	O(1) - V	0.26	0.30	0.04
Valley				
$D^{(,)}$ - $E^{(,)}$	V - O(2)	0.07	0.14	0.07
E – E’	O(2) - O(2)	0.00	0.10	0.10

* Note that the site definition can give only a rough orientation due to the size of NH_4.

Table 4

Energetics for oxygen diffusion from one site to an adjacent vacancy, see text. Initial and final states are each characterized by pairs of oxygen and oxygen vacancy sites, see Fig. 1. For each diffusion path corresponding differences ΔE in total energy and diffusion energies D for both path directions are listed, see text. All energies are shown in eV.

X - Y	**ΔE(X→Y)**	**D(X→Y)**	**D(Y→X)**
$O(2)/O(3)_{vac}$ - $O(3)/O(2)_{vac}$	0.04	0.61	0.57
$O(3')/O(3)_{vac}$ - $O(3)/O(3')_{vac}$	0.00	0.44	0.44
$O(2')/O(1)_{vac}$ - $O(1)/O(2')_{vac}$	1.40	1.40*	0.00*
$O(2)/O(1')_{vac}$ - $O(1')/O(2)_{vac}$	0.85	0.93	0.08
$O(3')/O(1')_{vac}$ - $O(1')/O(3')_{vac}$	0.44	1.38	0.94

* $D(Y \rightarrow X) < 10^{-3}$ eV from interpolations of the converged NEB path.

Table 5

Experimental and calculated hydrogen binding energies, $E_B(x)$, of NH_x, x = 1, … 4, in gas phase according to (6). The table includes results for the dissociation energy of the H_2 molecule, $E_B(H_2)$. All values are given in [eV].

Reaction $\mathbf{NH_x \rightarrow NH_{x-1} + H}$	**Experimental**	**Calculated**
x = 1	3.25[61]	3.71
x = 2	4.03[61]	4.20
x = 3	4.77[61]	4.77
x = 4	--	0.14
$E_B(H_2)$	4.52[62]	4.57

Table 6

Reaction energies computed for the dehydrogenation reaction of NH_x, see text. The theoretical gas phase values, $E_R^g(x)$ according to (8), are compared with values of $E_R^s(x)$ according to (10) for the perfect $V_2O_5(010)$ surface as well as for different oxygen vacancy sites of the reduced surface. All energies are given in [eV].

Reaction $NH_x \rightarrow NH_{x-1} + H$	**Gas phase**	**V_2O_5(010) perfect**	**$O(1)_{vac}$**	**$V/O(1')_{vac}$**	**$O(2)_{vac}$**	**$O(3)_{vac}$**
x = 1	1.43	0.36	1.94	1.81	1.77	1.72
x = 2	1.92	1.23	0.53	0.70	0.42	-0.21
x = 3	2.49	1.52	0.63	0.41	-1.63	-0.66
x = 4	-2.15	1.03	0.41	0.04	1.03	1.03

FIGURE CAPTIONS

Fig. 1. Cluster models used to evaluate (a) a specific surface NH_4 diffusion path, $V_{14}O_{45}H_{20}$, and (b) the path of O(3') oxygen diffusing to a neighboring O(3) vacancy site, $V_{16}O_{51}H_{24}$. Vanadium atoms are shown by large yellow, oxygen by smaller red, and saturating hydrogen by very small gray balls. Note that oxygen O(1') is hidden under a vanadium atom. The black dot in Fig. 1b denotes an oxygen vacancy $O(3)_{vac}$. Corresponding oxygen and vanadium sites are labeled accordingly.

Fig. 2. Diffusion paths and corresponding energetics for diffusion of atomic hydrogen at the perfect $V_2O_5(010)$ surface. Vanadium atoms are shown by large yellow and oxygen by smaller red balls. The diffusion paths of the three regions, ridge, slope, and valley, are indicated by black lines between equilibrium positions A, B, … K denoted by filled dots and transition state positions shown by open circles. At the bottom relative binding energies of hydrogen for the equilibrium and transition state sites along the paths are shown, see text.

Fig. 3. Initial, transition, and final state geometries for hydrogen diffusion paths (a) B → C (ridge), (b) E → F (valley), and (c) G → H (slope). Vanadium atoms are shown by large yellow, oxygen by smaller red balls, and hydrogen by small blue balls. The diffusion directions are indicated by blue arrows.

Fig. 4. Initial, transition, and final state geometries for surface H_2O formation starting with two OH groups at neighboring O(1) sites. Vanadium atoms are shown by large yellow, oxygen by smaller red balls, and hydrogen by small blue balls.

Fig. 5. Diffusion paths and corresponding energetics for diffusion of NH_4 at the perfect $V_2O_5(010)$ surface. Vanadium atoms are shown by large yellow and oxygen by smaller red balls. The diffusion paths of the three regions, ridge, slope, and valley, are indicated by black lines between equilibrium positions $A^{(')}$, $B^{(')}$, $C^{(')}$, $D^{(')}$, $E^{(')}$ denoted by filled dots and transition state positions shown by open circles. At the bottom relative binding energies of hydrogen for the equilibrium and transition state sites along the paths are shown, see text.

Fig. 6. (a) Initial, (b) transition, and (c) final state geometries for diffusive 'tumble' motion of NH_4 between positions A and B above neighboring O(1) sites at the ridge of the perfect V_2O_5(010) surface, see Fig. 5. The three snapshots are shown for top and side views with respect to the surface. Vanadium atoms are shown by large yellow, oxygen by smaller red balls, and hydrogen by small blue balls. The diffusion directions are indicated by blue arrows.

Fig. 7. (a) Initial, (b) transition, and (c) final state geometries for diffusive 'twist' motion of NH_4 between positions B and C above neighboring O(1) sites at the ridge of the perfect V_2O_5(010) surface. The three snapshots are shown for top and side views with respect to the surface. Vanadium atoms are shown by large yellow, oxygen by smaller red balls, and hydrogen by small blue balls. The diffusion directions are indicated by blue arrows.

Fig. 8. Energetics of the diffusion of oxygen from an O(3') site to a neighboring vacancy site $O(3)_{vac}$. The figure includes initial (denoted O(3')/$O(3)_{vac}$), transition, and final state geometries (denoted O(3)/$O(3')_{vac}$) along the diffusion path. Vanadium atoms are shown by large yellow, oxygen by smaller red balls, and oxygen vacancy sites are indicated by small black dots. Parameters a, b (in Å) refer to distances between the diffusing oxygen and its vanadium neighbors.

Fig. 9. Energetics of the diffusion of sub-surface oxygen from an O(1') site to a neighboring vacancy site $O(2)_{vac}$. The figure includes initial, transition, and final state geometries along the diffusion path. Vanadium atoms are shown by large yellow, oxygen by smaller red balls, and oxygen vacancy sites are indicated by small black dots.

Fig. 10. Energy diagrams of NH_x, x = 0,1, … 4, (de)hydrogenation from cluster calculations, see text. The diagrams are labeled accordingly and refer to reactions in gas phase (blue), at the V_2O_5(010) surface (black), and at the reduced V_2O_5(010) surface near oxygen vacancy sites $O(1)_{vac}$ (red), V/$O(1')_{vac}$ (purple dashed), $O(2)_{vac}$ (green), and $O(3)_{vac}$ (green dashed). All energies (in eV) are given relative to the value E_R^s(x=3) of NH_3 at the surface which set to zero.

FIGURES

Fig. 1

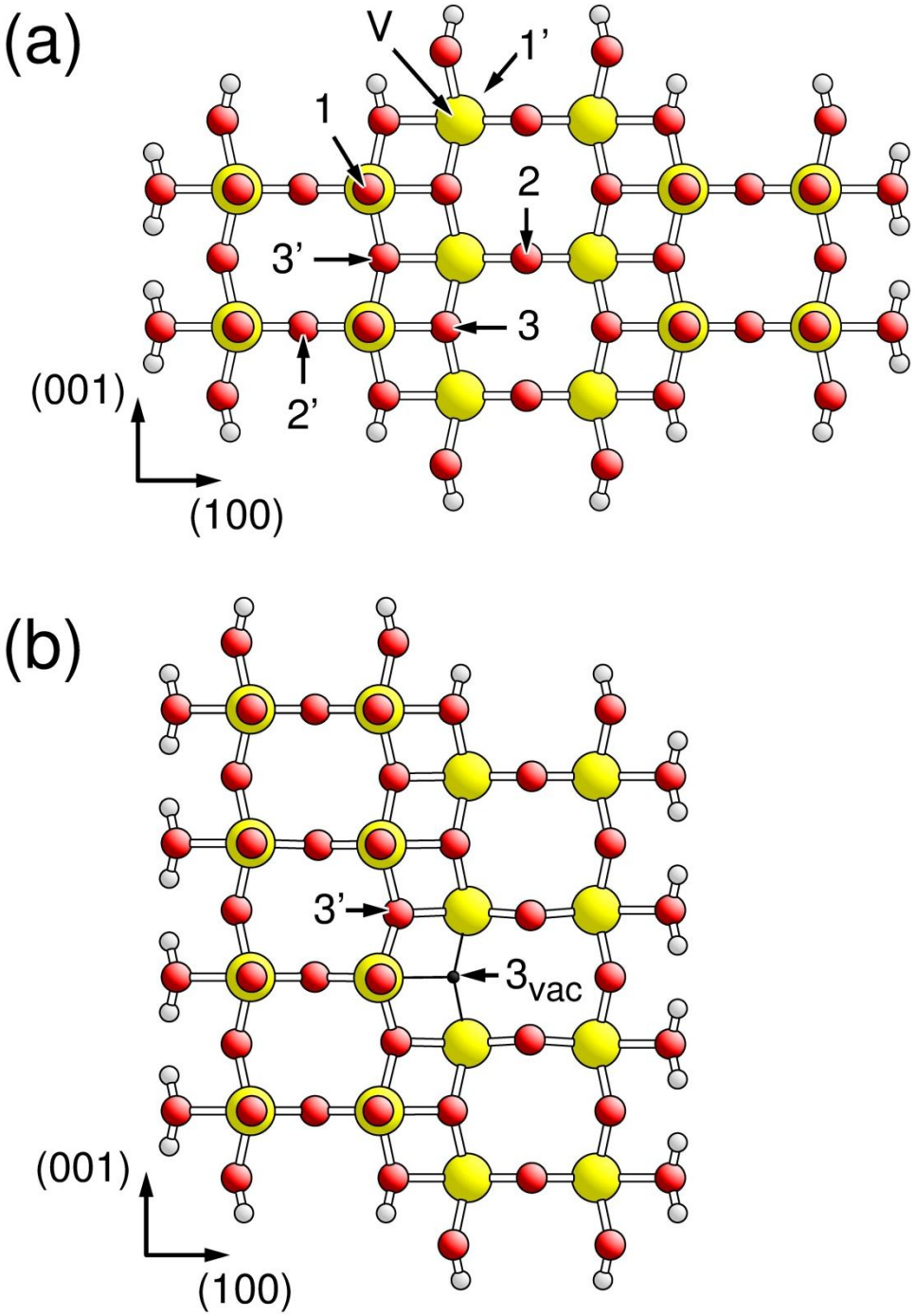

Fig. 2

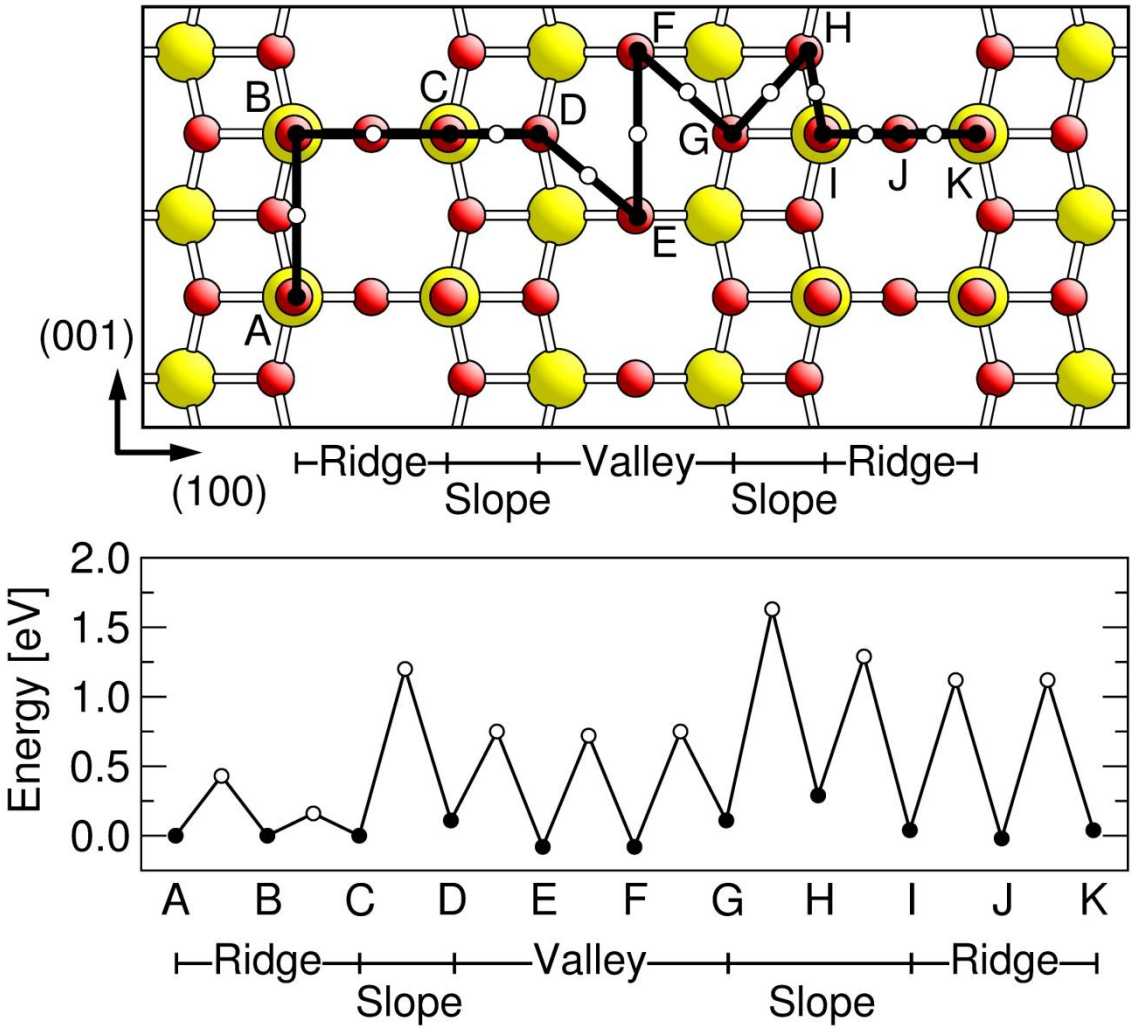
A
B
C
D
E
F
G
H
I
J
K
(001)
(100)
Ridge
Slope
Valley
Slope
Ridge
Energy [eV]
2.0
1.5
1.0
0.5
0.0
A B C D E F G H I J K
Ridge
Slope
Valley
Slope
Ridge

Fig. 3

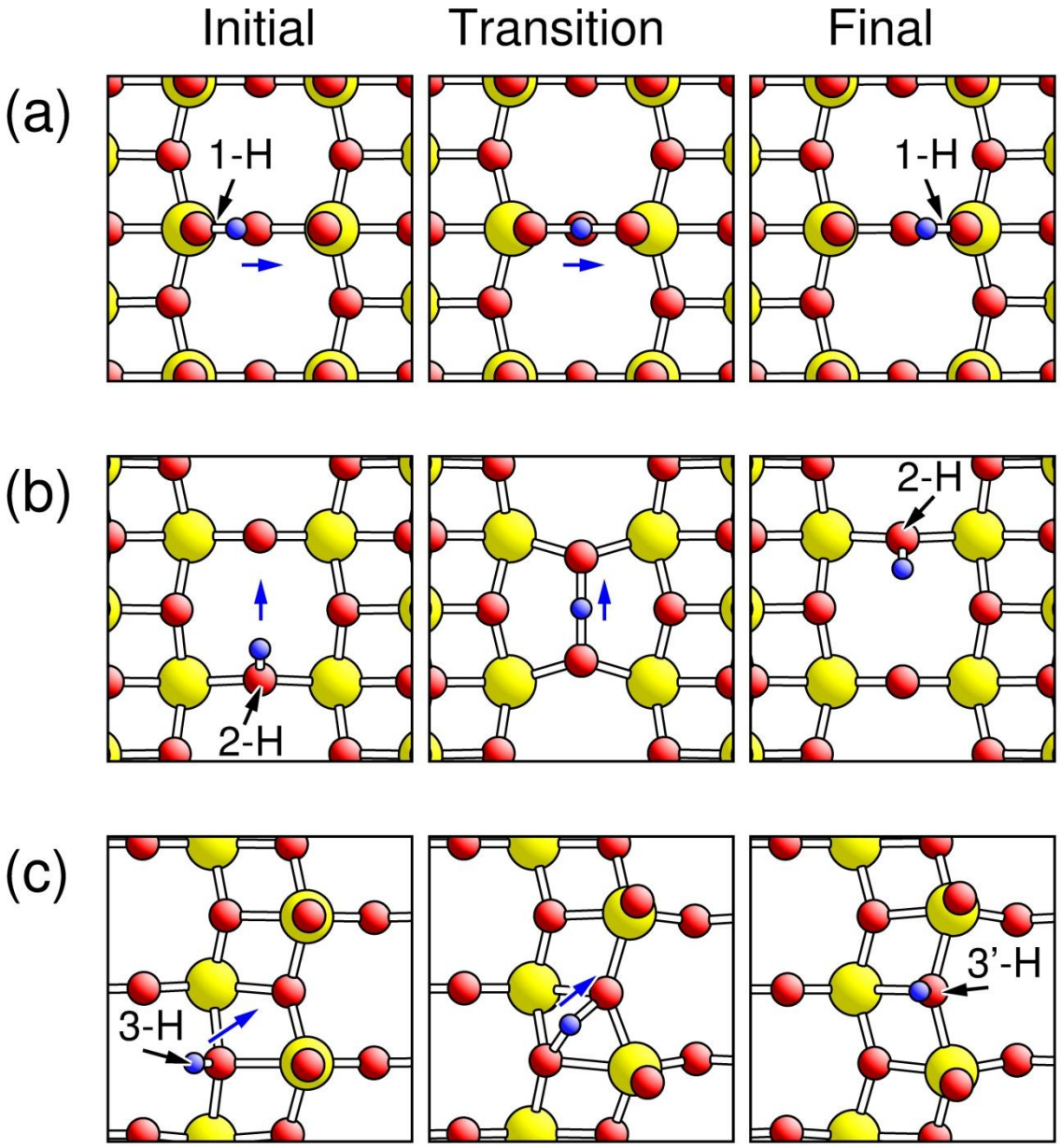

Fig. 4

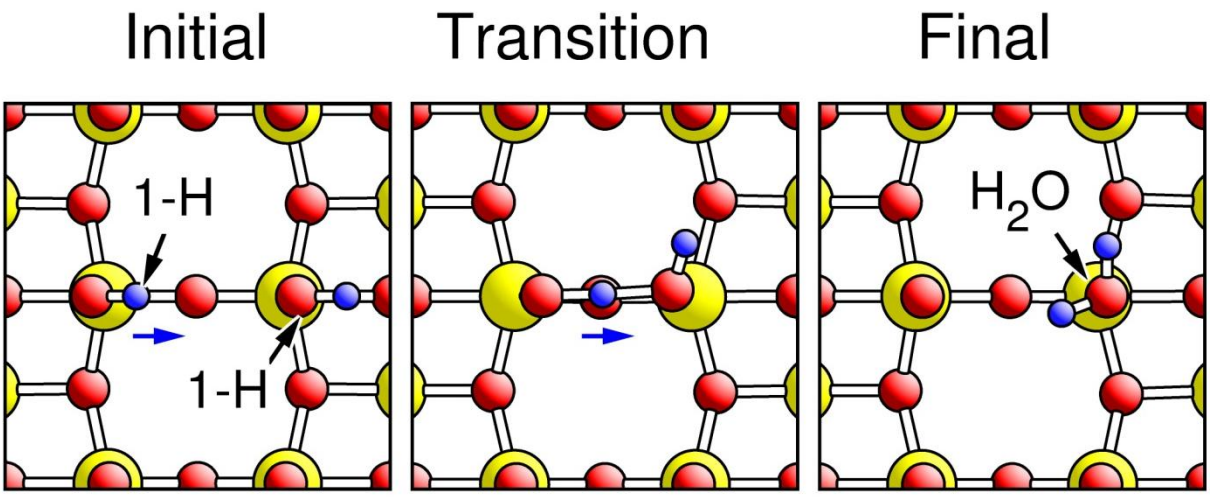

Fig. 5

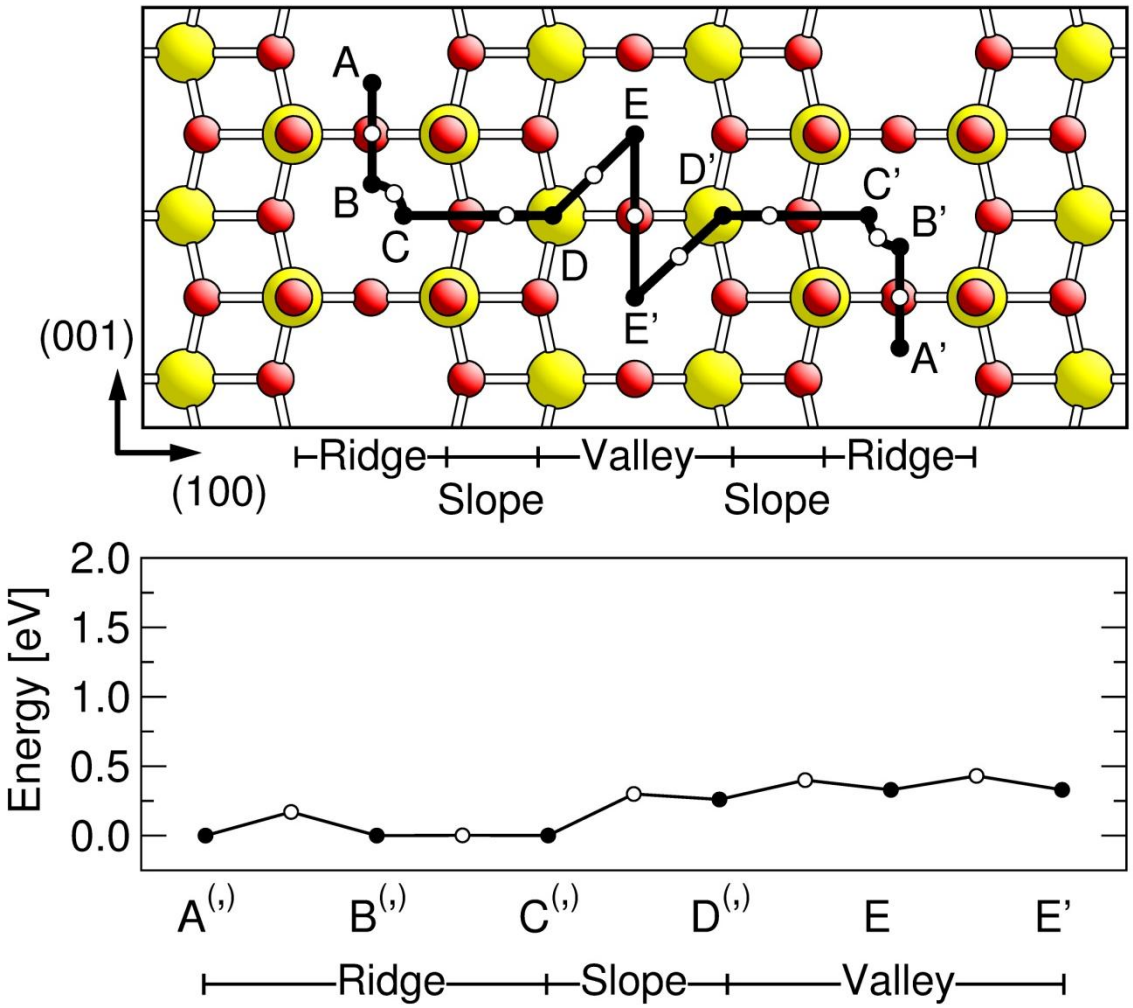
A
B
C
D
E
D'
C'
B'
A'
E'
(001)
(100)
Ridge
Slope
Valley
Slope
Ridge
Energy [eV]
2.0
1.5
1.0
0.5
0.0
A(,)
B(,)
C(,)
D(,)
E
E'
Ridge
Slope
Valley

Fig. 6

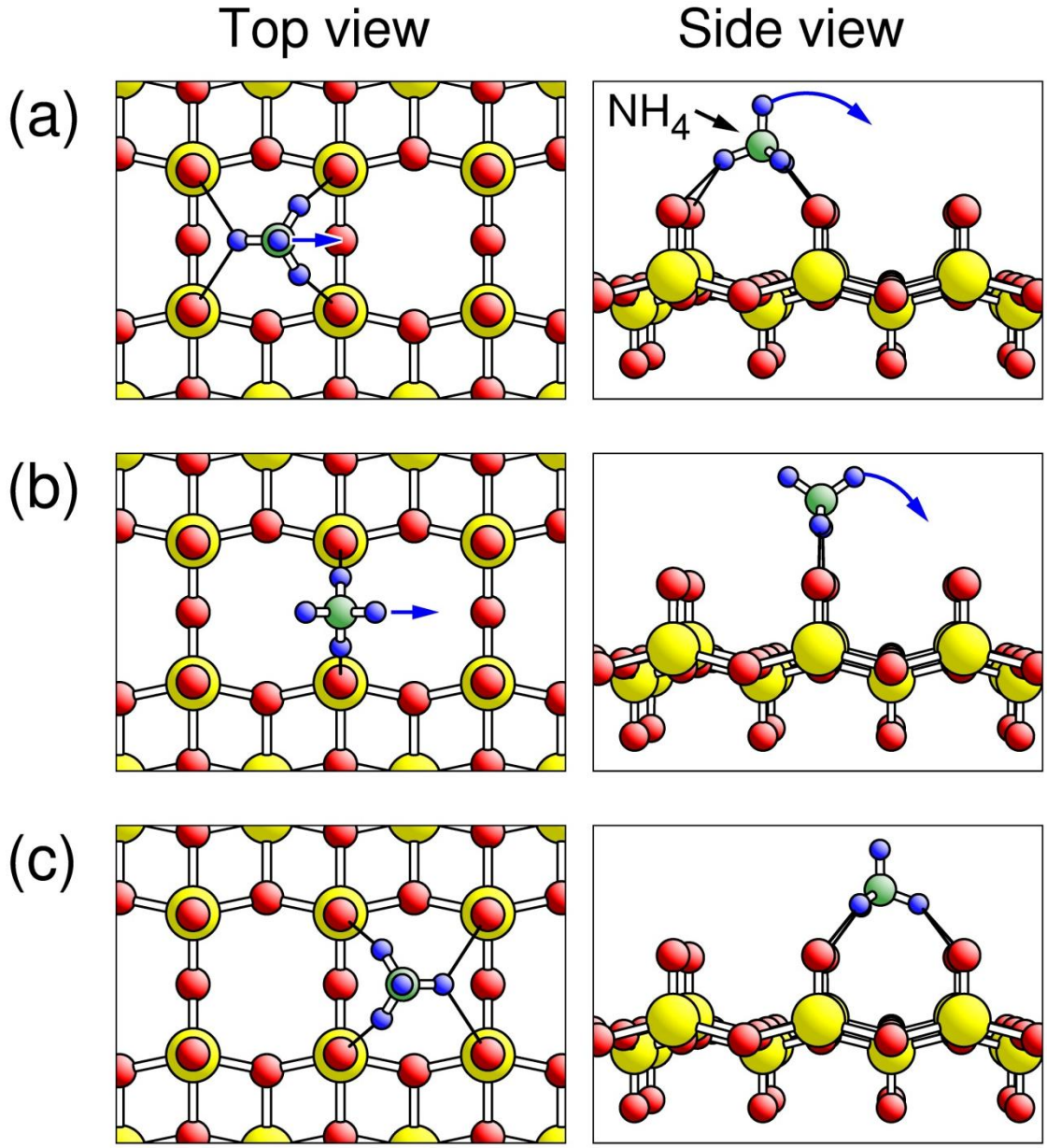

Fig. 7

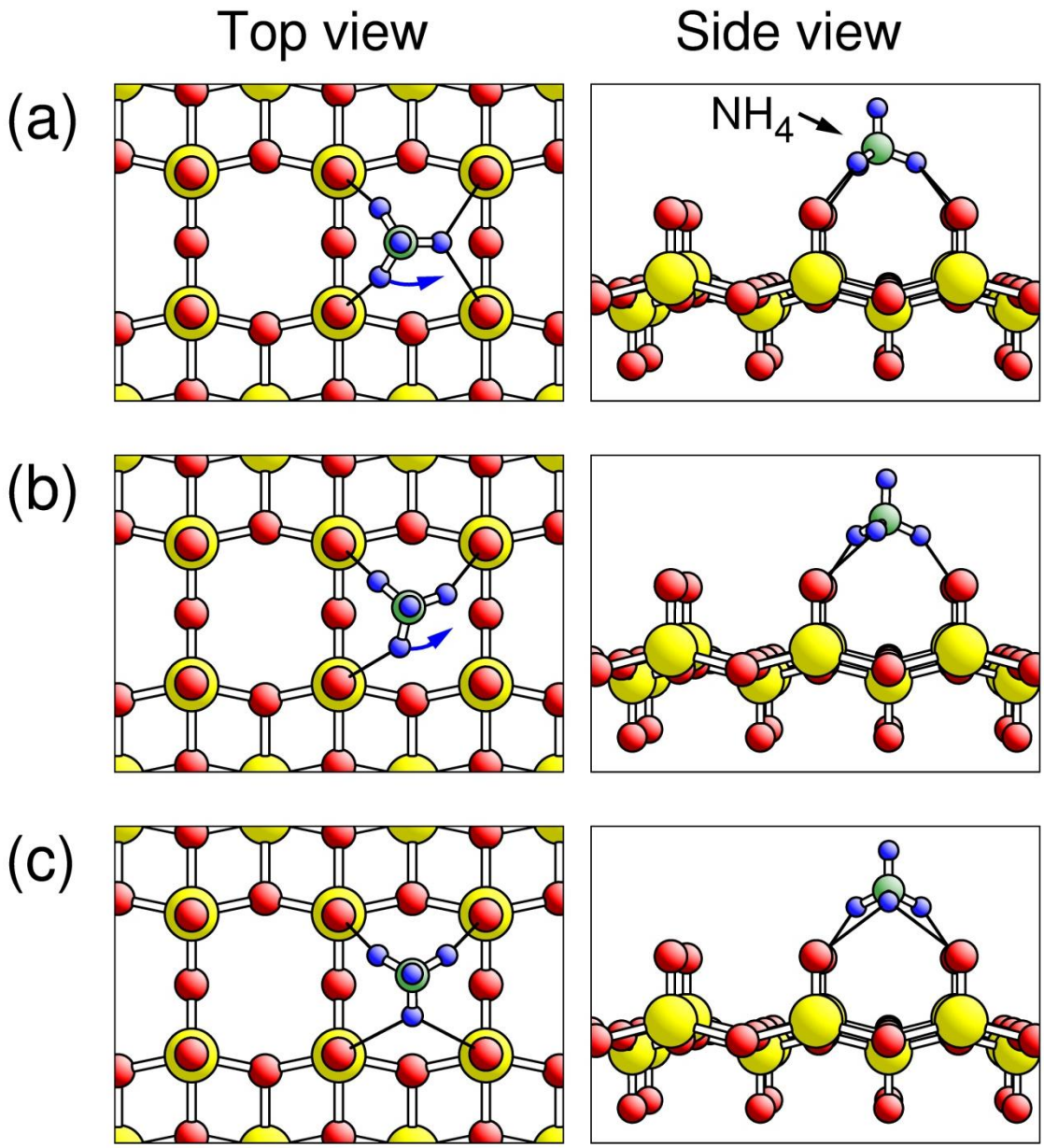

Fig. 8

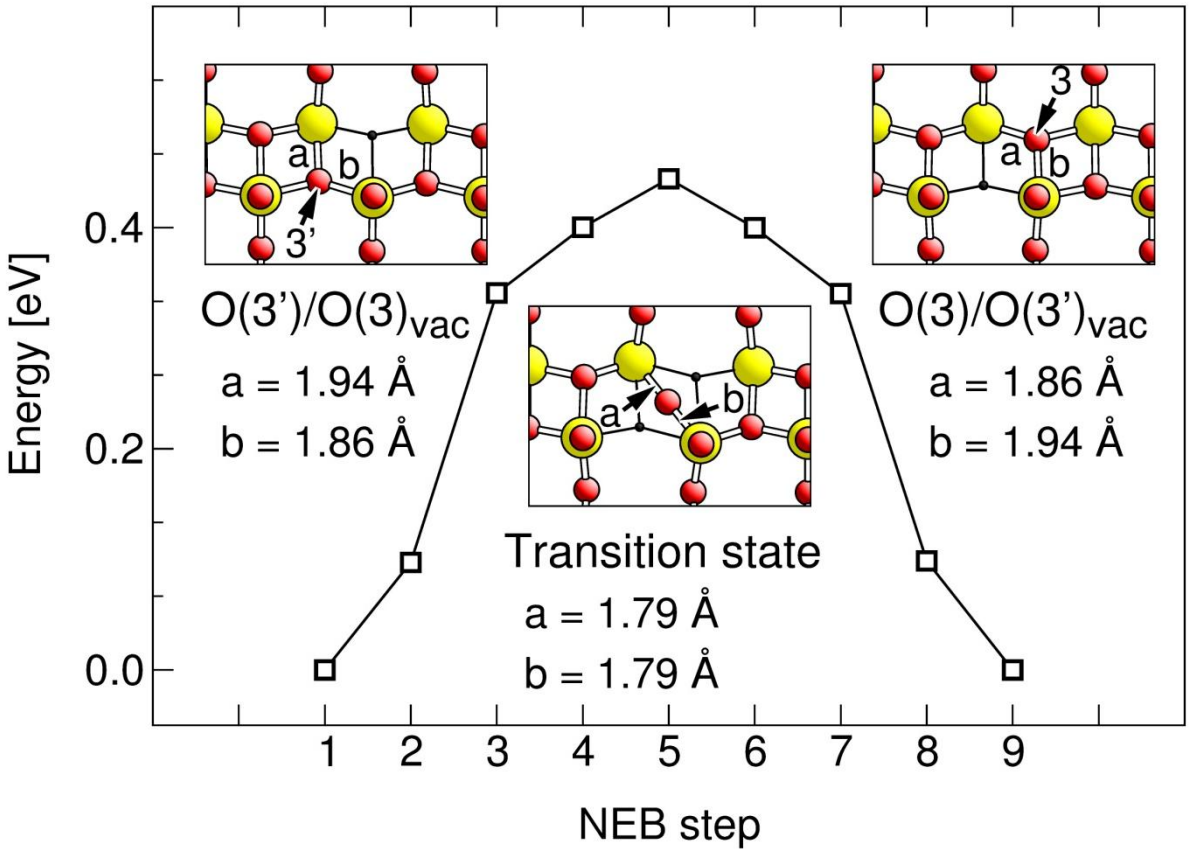
Energy [eV]
0.0
0.2
0.4
1
2
3
4
5
6
7
8
9
NEB step
a
b
3'
O(3')/O(3)vac
a = 1.94 Å
b = 1.86 Å
Transition state
a = 1.79 Å
b = 1.79 Å
3
O(3)/O(3')vac
a = 1.86 Å
b = 1.94 Å

Fig. 9

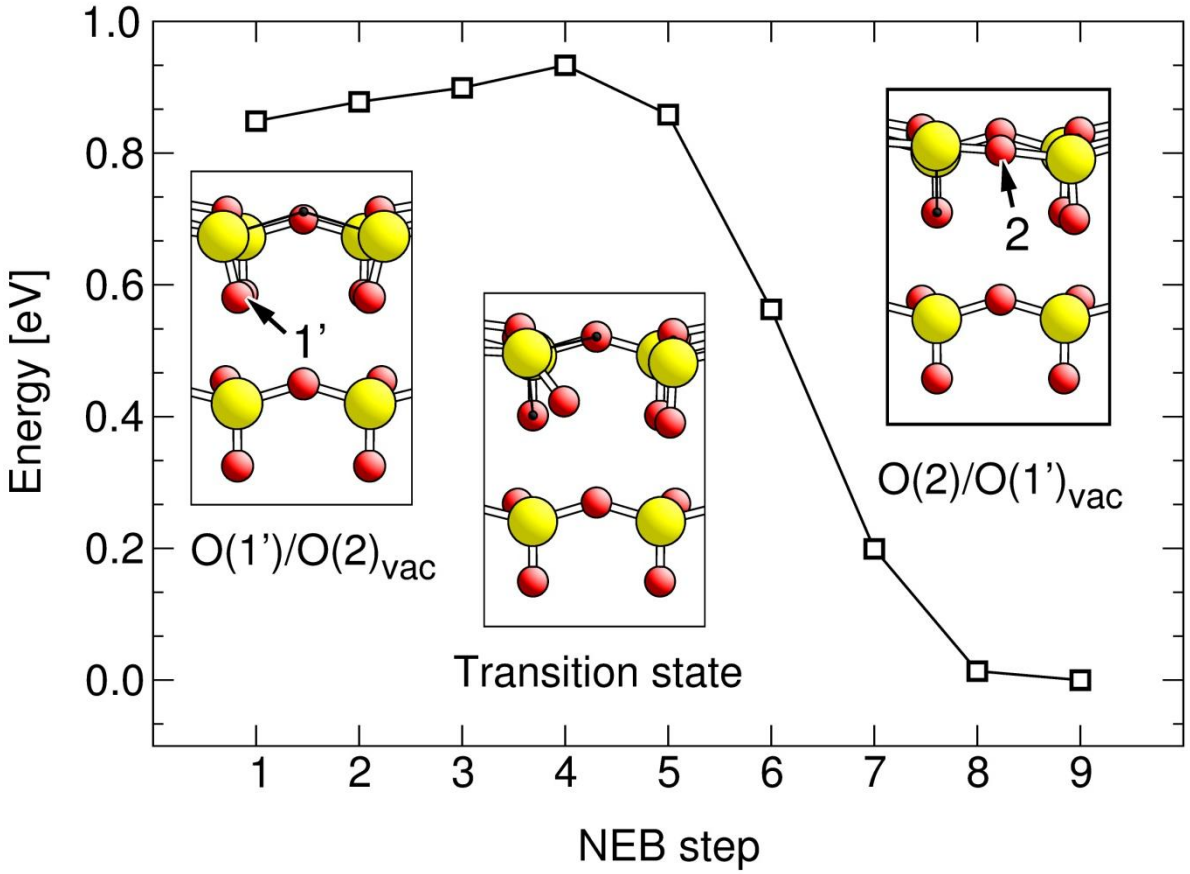
1.0
0.8
0.6
0.4
0.2
0.0
Energy [eV]
1
2
3
4
5
6
7
8
9
NEB step
1'
O(1')/O(2)vac
Transition state
2
O(2)/O(1')vac

Fig. 10

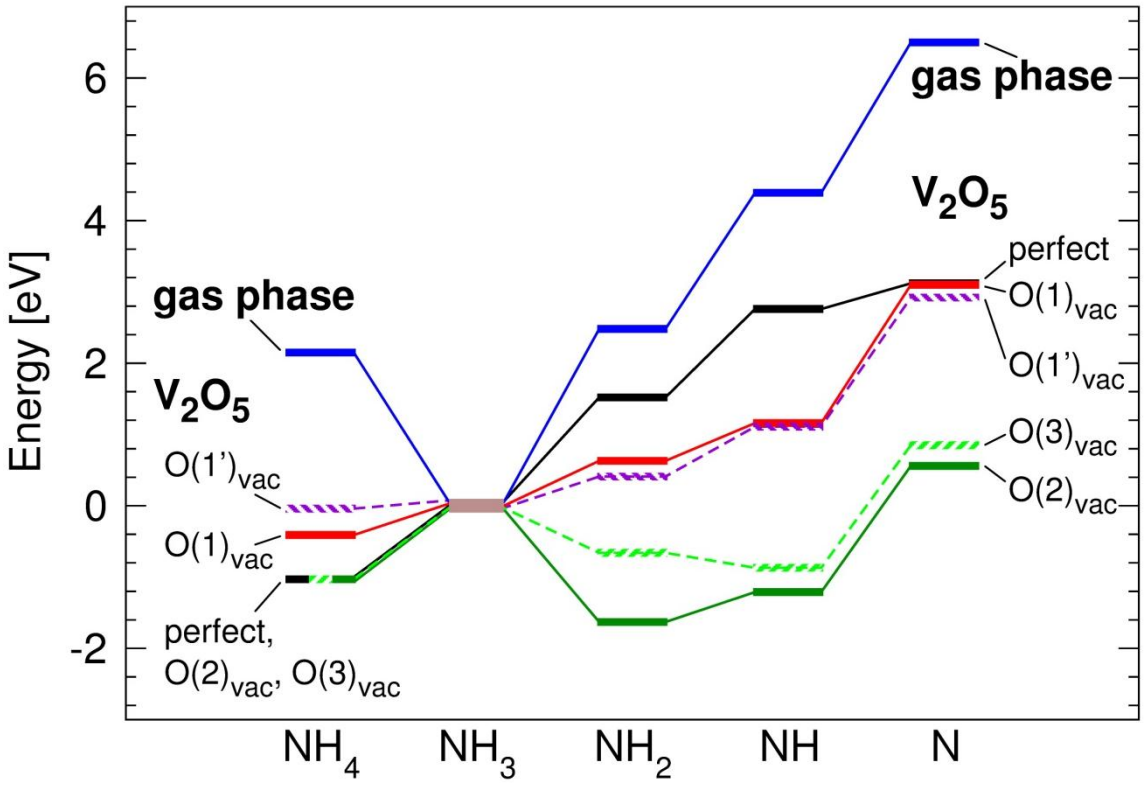
Energy [eV]
6
4
2
0
-2
gas phase
V2O5
O(1')vac
O(1)vac
perfect,
O(2)vac, O(3)vac
gas phase
V2O5
perfect
O(1)vac
O(1')vac
O(3)vac
O(2)vac
NH4
NH3
NH2
NH
N